Enthalpies of Oxidation of $CaMnO_{3-\delta}$, $Ca_2MnO_{4-\delta}$ and $SrMnO_{3-\delta}$ — Deduced Redox Properties

Lisbeth Rørmark,[†,‡] Anne Beate Mørch,[‡] Kjell Wiik,[†] Svein Stølen,[‡] and Tor Grande*[,†]

Department of Chemistry, Norwegian University of Science and Technology, N-7491 Trondheim, Norway, and Department of Chemistry, University of Oslo, Postbox 1033, N-0315 Oslo, Norway

Received February 21, 2001. Revised Manuscript Received April 30, 2001

The enthalpies of oxidation of $CaMnO_{3-\delta}$, $Ca_2MnO_{4-\delta}$, and $SrMnO_{3-\delta}$ have been determined by in situ oxidation in a high-temperature adiabatic calorimeter. $CaMnO_3$, Ca_2MnO_4, and $SrMnO_3$ were synthesized by the EDTA precursor or the ceramic method, and partly reduced materials were prepared by topotactic reduction in diluted H_2 (5−10%) at 290−355 °C. Unit cell dimensions and oxygen stoichiometry of partly reduced and reoxidized materials were determined by powder X-ray diffraction, thermogravimetry, and iodometric titration. The enthalpy of oxidation of $SrMnO_{3-\delta}$ was considerably less exothermic than the corresponding value for $CaMnO_{3-\delta}$, and the enthalpy of oxidation of $Ca_2MnO_{4-\delta}$ was more exothermic than for $CaMnO_{3-\delta}$. The enthalpy of oxidation is discussed in terms of the basicity of oxides, the Goldschmidt tolerance factor, and the crystal structures of the oxidized and reduced materials. Finally, based on the enthalpy of oxidation, the oxygen defect chemistry of these materials is estimated using simple thermodynamic models. Using the measured enthalpy of oxidation and estimated entropy of oxidation, the measured oxygen nonstoichiometry is reproduced rather well. A free fit of the same models to the experimental data gives enthalpies of oxidation that are far more exothermic than the measured values. The present findings demonstrate that simple models based on point defect equilibrium may give significant errors in the enthalpy and entropy of formation of point defects, despite a good fit to the free energy.

Introduction

Perovskites based on solid solutions of $LaMnO_{3\pm\delta}$ and $AMnO_{3-\delta}$ (A = Ca, Sr) have been widely studied because of their potential as cathodes in solid oxide fuel cells (SOFC).[1−3] Recently, these materials have also received considerable attention due to their magnetoresistance.[4,5] Despite the considerable interest, the thermodynamic properties of the solid solutions have not been thoroughly investigated. For all these potential applications the valence state of manganese is of importance, and a fundamental understanding of the defect chemistry and nonstoichiometry is necessary. Their chemical stability has also been addressed due to reactions with the electrolyte (cubic stabilized zirconia) in SOFC.[6,7] Yokokawa et al.[8−10] have previously offered a review on the thermodynamic properties of the end members of $La_{1-x}A_xMnO_{3\pm\delta}$, but most of these data are estimated.

The crystal structure of orthorhombic $Ca_2Mn_2O_5$ (a = 5.424 Å, b = 10.230 Å, and c = 3.735 Å) is related to the perovskite structure, where O-vacancies are evenly distributed and Mn^{3+} cations have square pyramidal coordination.[11] At around 285 ± 10 °C[16] $Ca_2Mn_2O_5$ oxidizes rapidly to orthorhombic $CaMnO_{3.0}$ with the space group *Pnma* (a = 5.279 Å, b = 7.448 Å, and c = 5.264 Å).[11,12] $CaMnO_{3-\delta}$ ($2.85 \leq 3 - \delta \leq 3.00$) has been found to be an n-type semiconductor.[13,14] Reller et al.[15] have reported the oxygen vacancy ordered phases $CaMnO_{2.556}$, $CaMnO_{2.667}$, $CaMnO_{2.75}$, and $CaMnO_{2.8}$. The

* Corresponding author. Address: Department of Chemistry, NTNU, Sem Sælandsvei 12, N-7491 Trondheim, Norway. Telephone: +47 73 59 40 84. Fax: +47 73 59 08 60. E-mail: tor.grande@chembio.ntnu.no.
† Norwegian University of Science and Technology.
‡ University of Oslo.

(1) Takeda, Y.; Nakai, S.; Kojima, T.; Kanno, R.; Imanishi, N.; Shen, G. Q.; Yamamoto, O.; Mori, M.; Asakawa, C.; Abe, T. *Mater. Res. Bull.* **1991**, *26*, 153.
(2) Hammouche, A.; Siebert, E.; Hammou, A. *Mater. Res. Bull.* **1989**, *24*, 367.
(3) Faaland, S.; Knudsen, K. D.; Einarsrud, M. A.; Rørmark, L.; Høier, R.; Grande, T. *J. Solid State Chem.* **1998**, *140*, 320.
(4) Mahendiran, R.; Tiwary, S. K.; Raychaudhuri, A. K.; Ramakrishnan, T. V.; Mahesh, R.; Rangavittal, N.; Rao, C. N. R. *Phys. Rev. B* **1996**, *53*, 3348.
(5) Mahesh, R.; Mahendiran, R.; Raychaudhuri, A. K.; Rao, C. N. R. *J. Solid State Chem.* **1995**, *114*, 297.
(6) Brugnoni, C.; Ducati, U.; Scagliotti, M. *Solid State Ionics* **1995**, *76*, 177.
(7) Taimatsu, H.; Wada, K.; Kaneko, H.; Yamamura, H. *J. Am. Ceram. Soc.* **1992**, *75*, 401.
(8) Yokokawa, H.; Sakai, N.; Kawada, T.; Dokiya, M. *Denki Kagaku* **1989**, *57*, 821.
(9) Yokokawa, H.; Sakai, N.; Kawada, T.; Dokiya, M. *Denki Kagaku* **1989**, *57*, 829.
(10) Yokokawa, H.; Sakaki, N.; Kawada, T.; Dokiya, M. *Denki Kagaku* **1990**, *58*, 162.
(11) Poeppelmeier, K. R.; Leonowicz, M. E.; Scanlon, J. C.; Longo, J. M. *J. Solid State Chem.* **1982**, *45*, 71.
(12) Poeppelmeier, K. R.; Leonowicz, M. E.; Longo, J. M. *J. Solid State Chem.* **1982**, *44*, 89.
(13) Taguchi, H. *Phys. Status Solidi A* **1985**, *88*, K79.
(14) Taguchi, H.; Sonoda, M.; Nagao, M. *J. Solid State Chem.* **1998**, *137*, 82.
(15) Reller, A.; Thomas, J. M.; F. R. S.; Jefferson, D. A.; Uppal, M. K. *Proc. R. Soc. London* **1984**, *A 394*, 223.
(16) Rørmark, L.; Stevens, R.; Boerio-Goates, J.; Wiik, K.; Stølen, S.; Grande, T., submitted to *J. Chem. Thermodynamics*.

10.1021/cm011050l CCC: $20.00
Published on Web 10/12/2001

lattice parameters of tetragonal $CaMnO_{2.8}$ were $a = b = 8.34$ Å and $c = 7.46$ Å, and those of orthorhombic $CaMnO_{2.75}$ were $a = 5.35$ Å, $b = 10.50$ Å, and $c = 7.46$ Å.[15]

Tetragonal Ca_2MnO_4 with space group I_1/acd ($a = 5.183$ Å and $c = 24.117$ Å) has the K_2NiF_4 structure with alternating $CaMnO_3$ perovskite and CaO rock salt layers.[17] The reduced $Ca_2MnO_{3.5}$, with Mn^{3+} cations in square-pyramidal coordination, is orthorhombic with space group *Bbcm* ($a = 5.30$ Å, $b = 10.05$ Å, and $c = 12.23$ Å). $Ca_2MnO_{3.5}$ is easily oxidized to Ca_2MnO_4 at around 300 °C.[12]

Orthorhombic $Sr_2Mn_2O_5$ with space group *Pbam* or *Pba*2 ($a = 5.523$ Å, $b = 10.761$ Å, and $c = 3.811$ Å) is isostructural to $Ca_2Mn_2O_5$.[18] $Sr_2Mn_2O_5$ oxidizes easily to cubic perovskite $SrMnO_{3.0}$ with $a = 3.806$ Å,[19] and the oxidation is initiated at 180 ± 10 °C in air.[16] Metastable $SrMnO_3$ perovskite transforms to the stable hexagonal $SrMnO_3$ at 800 °C. Hexagonal $SrMnO_3$ is stable up to about 1400 °C, where it transforms to the high-temperature perovskite phase.[19] The crystal structure of hexagonal $SrMnO_3$ consists of pairs of MnO_6 octahedra sharing faces. Neighboring pairs are linked by sharing corners, giving a 3D network. Both the hexagonal and the perovskite phase of $SrMnO_3$ has been found to be semiconducting.[20,21]

We have recently started a program to investigate the thermodynamic properties of the solid solutions $La_{1-x}A_xMnO_{3\pm\delta}$ (A = Ca, Sr, $0 \le x \le 1$). Here, we report on the enthalpies of oxidation of $Ca_2Mn_2O_5$, $Ca_2MnO_{3.5}$, and $Sr_2Mn_2O_5$. We also apply the enthalpies of oxidation to describe the defect chemistry based on a simple solution model. In addition, measurements of heat capacities of $Ca_2Mn_2O_5$ and $Sr_2Mn_2O_5$ by adiabatic calorimetry,[16] enthalpies of formation of $La_{1-x}A_xMnO_{3\pm\delta}$ by high-temperature solution calorimetry,[22] and finally studies of phase diagrams and oxygen nonstoichiometry[23] are reported in separate papers.

Experimental Procedure

Synthesis. The samples labeled $CaMnO_3$(A) and Ca_2MnO_4-(A) were prepared by the ceramic method. Stoichiometric amounts of $CaCO_3$ (>99%, Fluka) and Mn_3O_4 were mixed by mortaring and heat-treated at 1000 °C for 24 h. The powders were then hand milled, pressed into pellets, and calcined in air at 1200 °C for 24 h. Mn_3O_4 was prepared from $MnCO_3 \cdot xH_2O$ (>99%, Fluka) by heat treatment at 1050 °C for 24 h.

The samples labeled $CaMnO_3$(B) and $SrMnO_3$(B) were synthesized by the EDTA precursor method. $Ca(NO_3)_2 \cdot 4H_2O$ (>99.0%, Merck), $Sr(NO_3)_2$ (>99%, Merck), and $Mn(NO_3)_2 \cdot 4H_2O$ (>98.5%, Merck) were heat-treated at temperatures between 700 and 1100 °C to determine the exact amount of crystal water in the nitrates. Stoichiometric amounts of nitrates were dissolved in ion-exchanged water, then an EDTA (ethylendiamine-tetraacetic acid, 99.7%, Sigma) solution (0.8 M and pH 8−9) was added, and the final solution was heated on a hot plate to 80 ± 3 °C. The solution was continuously stirred at 80 °C until a gel was formed. The pH was controlled during heating, and NH_3 (concentrated) was added to keep the pH at 7−11, depending on the type of ions in the solution. The gel was dried overnight at 150−200 °C and fired at approximately 500 °C to remove all the organic matter. $CaMnO_3$-(B) was calcined in air at 1100 °C for 72 h and at 1200 °C for 96 h with heating and cooling rates of 100 °C/h. $SrMnO_3$(B) was first calcined at 1100 °C for 72 h. This gave the hexagonal phase that is stable below 1400 °C in air.[19] To achieve the metastable perovskite $SrMnO_{3-\delta}$, the powder was heat-treated in air at 1525 °C for 1−2 h and air-quenched. This gave the perovskite phase surrounded by a thin layer of the hexagonal phase due to oxidation during cooling. These two phases were easily separated due to color differences, and all further handling and measurements were performed on the metastable perovskite phase of $SrMnO_3$(B).

All samples were subjected to reduction (topotactic) in either 10% H_2 in Ar (A samples) or 5% H_2 in N_2 (B samples) aiming for a complete reduction of Mn to three valent. $CaMnO_3$(A) and Ca_2MnO_4(A) were reduced at 300 and 355 °C, respectively, for 7 days. The perovskites $CaMnO_3$(B) and $SrMnO_3$(B) were reduced at 305 and 290 °C, respectively; the duration of the reduction varied between 2 and 5 weeks, and the amount of sample was 22−25 g. During reduction of the B samples the mass of the samples was measured in situ using a balance. This made it possible to reduce the oxygen stoichiometry of the samples to close to 2.5. The reduction of $CaMnO_3$ has previously been described by Poeppelmeier.[11,12] The same method was applied for the metastable perovskite $SrMnO_3$-(B), previously not described in the literature. The initiation temperature for the reduction of $SrMnO_3$(B) was observed at 290 °C by thermogravimetry.

Characterization of Materials. The oxygen stoichiometry of the reduced samples was calculated from the mass gained during the measurement of the enthalpy of oxidation, assuming the oxidized samples to be stoichiometric. In addition, the oxygen stoichiometry of the reduced and reoxidized samples was verified (A samples) or determined (B samples) by thermogravimetry (Perkin-Elmer TGS2 or TGA 7, Perkin-Elmer Corp.) and iodometry.

Sample sizes of 30−50 mg (TGS 2) or 5−15 mg (TGA 7) were used in the thermogravimetric analysis. $CaMnO_{3-\delta}$(A), $CaMnO_{3-\delta}$(B), $Ca_2MnO_{4-\delta}$(A), and $SrMnO_{3-\delta}$(B) were heated to 600, 700, 500, and 500 °C in synthetic air, respectively, where they became stoichiometric. The oxygen stoichiometry of the reduced samples was then calculated from the increased mass due to oxidation.

Iodometric titration was performed on 10−30 mg of sample. The sample was weighed out in an ampule or round-necked vessel. An excess of potassium iodide (KI) and some distilled water were added. The solution was flushed with Ar or N_2 to avoid air-oxidation of excess I^-. Some hydrochloric acid was added, and then the ampule/vessel was closed and heated for the sample to dissolve. The solution was cooled and titrated with standardized sodium thiosulfate. Starch was used as an indicator. This gave the mean valency of manganese, and the amount of oxygen was then calculated.

Crystalline phases in the powders were identified by X-ray diffraction (SIEMENS D5000 or D5005, Siemens Germany) using Cu Kα radiation. Silicon was used as an internal standard in order to determine the unit cell parameters.

Adiabatic Calorimetry. The high-temperature adiabatic calorimetric apparatus and the measuring technique have been described earlier by Grønvold[24] and Stølen et al.[25]

For the measurement of the oxidation enthalpy, samples of 19−30 g were contained in an open vitreous silica container. The volume of the container that fits tightly into the calorimeter is about 40 cm^3. A central well in the container serves for

(17) Leonowicz, M. E.; Poeppelmeier, K. R.; Longo, J. M. *J. Solid State Chem.* **1985**, *59*, 71.
(18) Caignaert, V.; Nguyen, N.; Hervieu, M.; Raveau, B. *Mater. Res. Bull.* **1985**, *20*, 479.
(19) Negas, T.; Roth, R. S. *J. Solid State Chem.* **1970**, *1*, 409.
(20) Kuroda, K.; Shinozaki, K.; Uematsu, K.; Mizutani, N.; Kato, M. *J. Am. Ceram. Soc.* **1980**, *63*, 109.
(21) Kikuchi, K.; Chiba, H.; Kikuchi, M.; Syono, Y. *J. Solid State Chem.* **1999**, *146*, 1.
(22) Rørmark, L.; Wiik, K.; Stølen, S.; Grande, T. *J. Solid State Chem.* in print.
(23) Rørmark, L.; Wiik, K.; Stølen, S.; Grande, T. *J. Mater. Chem.* in print.
(24) Grønvold, F. *Acta Chem. Scand.* **1967**, *21*, 1695.
(25) Stølen, S.; Glöckner, R.; Grønvold, F. *J. Chem. Thermodyn.* **1996**, *28*, 1263.

the heater and the platinum resistance thermometer. The calorimeter is heated in a stepwise fashion, and electrically heated and electronically controlled adiabatic shields surround the calorimeter proper. A guard shield system is outside the adiabatic shield and the whole assembly is placed in a vertical tube furnace. The calorimeter, shields, and guard are all made of silver.[24]

The temperature was measured with an ASL F-18 resistance bridge using locally constructed 25 Ω platinum resistance thermometers. Temperature calibration is performed according to the recommendation of ITS-90 to 933.473 K, and the temperature-resistance relationship is extrapolated to 1000 K. The accuracy in temperature determination is considered to be within ±0.02 K to 903 K, and within ±0.10 K above 903 K. The temperature resolution is $\approx 3 \times 10^{-5}$ K.[25]

Energy is supplied electrically by a constant current source. The current through the heater is measured every 10 s and the potential drop across the heater every second in between. The potential is measured using an 8.5 digit Hewlett-Packard digital voltmeter. The current is determined by measuring the potential drop over a calibrated resistor. The total time, as well as the triggering of the potential and current measurements, is measured or controlled using a Keithley counter.[25]

The total heat capacity of the system (calorimeter plus contents), $C_{P,\mathrm{tot}}$, and the enthalpy of oxidation are determined from accurately determined quantities of electrical energy (converted to heat in the central well of the calorimeter) and the temperature rise observed. Incomplete adiabatic conditions will always give rise to an enthalpy leak that must be taken into account. The enthalpy leak is determined by the temperature drift rates in the equilibrium periods preceding and following the input. The instrumental temperature drift rate is determined by the set points of the PID regulators giving power to the shield heaters. The set points are not changed in the temperature region where the oxidation takes place. There are three contributions to the energy account:

(1) the total energy supplied electrically to the calorimeter during heating from a given starting temperature to a specific end temperature, $\Delta_{\mathrm{input}}H$;

(2) the total enthalpy released by the sample during the oxidation process; and

(3) the enthalpy leak due to incomplete adiabatic conditions, $\Delta_{\mathrm{drift}}H$.

The enthalpy of oxidation, hence, can be determined from the observed temperature rise and the first and the third of the contributions given above. Since we determine the total heat capacity of the calorimeter with sample, $C_{P,\mathrm{tot}}$, the enthalpy needed to heat the sample from the start to the end temperature is given. The enthalpy released during the oxidation process is then determined as the difference between this energy and the total energy supplied to the calorimeter during the heating. A correction for the enthalpy leak is then done.

Correction of the difference in heat capacity of the vitreous silica reference ampule and the one used for a specific sample is applied. The difference in mass between different ampules is usually within 2 g, i.e., 0.03 mol of vitreous silica, which implies a correction of not more than 2 J/(K mol). The heat capacity of the vitreous silica used will be reported elsewhere (unpublished results). The uncertainty of the heat capacity of SiO_2 (vitreous) is within 0.3%.

Results

The experimental data are summarized in Table 1. The enthalpies of oxidation of $CaMnO_{3-\delta}$(A and B), $Ca_2MnO_{4-\delta}$(A), and $SrMnO_{3-\delta}$(B) are summarized in Table 2. The enthalpies of oxidation of the materials are calculated by the equation

$$\Delta_{\mathrm{ox}}H = (\Delta_{\mathrm{input}}H - \Delta_{\mathrm{total}}H + \Delta_{\mathrm{drift}}H)/n_{\mathrm{O_2}} \qquad (1)$$

where $\Delta_{\mathrm{input}}H$ is the total energy supplied electrically during oxidation, $\Delta_{\mathrm{total}}H$ is the total enthalpy needed to heat the sample from T_{start} to T_{end}, $\Delta_{\mathrm{drift}}H$ is the enthalpy leak due to incomplete adiabatic conditions, and $n_{\mathrm{O_2}}$ is the amount of oxygen consumed in the oxidation reaction. The total heat capacity of the system (calorimeter plus content) for the $CaMnO_{3-\delta}$(B) sample is shown in Figure 1. The line shown in the figure is the fitted heat capacity used in the calculations of $\Delta_{\mathrm{total}}H$. A typical example of the measured temperature drift rate (TDR) is shown for the oxidation of $CaMnO_{3-\delta}$(B) in Figure 2. The filled circles represent the observed TDR during oxidation, while the crosses show the TDR, for several samples, when no oxidation occurs. The start and end temperatures of the oxidation are determined by the increase and decrease in the TDR and are given by arrows in Figure 2. By adjusting the set points in a way that secures a low temperature drift rate (TDR) in the temperature region of interest, the drift enthalpy given in Table 1 becomes small. However, since the temperature variation of the TDR is well-defined, a slightly higher instrumental temperature

Table 1. Experimental Data for Calculation of the Enthalpies of Oxidation

sample	temp of oxidation start (K)	temp of oxidation end (K)	$\Delta_{\mathrm{input}}H$ (J)	$\Delta_{\mathrm{total}}H$ (J)	$\Delta_{\mathrm{drift}}H$ (J)	gained mass (g)
$CaMnO_{3-\delta}$(A)	420.834	634.454	16 018	22 967	−404	0.72441
$CaMnO_{3-\delta}$(B)	402.207	631.991	11 426	23 299	98	1.05912
$Ca_2MnO_{4-\delta}$(A)	429.816	669.250	15 636	24 524	−47	0.64606
$SrMnO_{3-\delta}$(B)	328.240	533.894	11 943	18 765	−80	0.75498

Table 2. Oxygen Stoichiometry for Reduced and Reoxidized Samples, the Change in Oxygen Stoichiometry during Oxidation, $\Delta\delta$, and the Enthalpies of Oxidation of $CaMnO_{3-\delta}$(A and B), $Ca_2MnO_{4-\delta}$(A) and $SrMnO_{3-\delta}$(B)[a]

sample	oxygen stoichiometry reduced	oxygen stoichiometry oxidized	$\Delta\delta$	enthalpy of oxidation kJ/mol of O_2	enthalpy of oxidation kJ/mol of Mn
$CaMnO_{3-\delta}$(A)	2.77	3.00	0.23	325 ± 11	81.3 ± 2.8
$CaMnO_{3-\delta}$(B)	2.53 ± 0.01[b]	2.99 ± 0.01[b]	0.46	356 ± 7	89.0 ± 1.6
$Ca_2MnO_{4-\delta}$(A)	3.65	4.00	0.35	443 ± 12	110.8 ± 3.0
$SrMnO_{3-\delta}$(B)	2.57 ± 0.01	2.99 ± 0.01	0.42	293 ± 10	73.3 ± 2.5

[a] The maximum error in the oxygen stoichiometry of the B samples is ±0.01. [b] The oxygen stoichiometry of $CaMnO_{3-\delta}$(B) was estimated assuming that the reduced sample contained 1.49 wt % $CaMn_2O_4$.

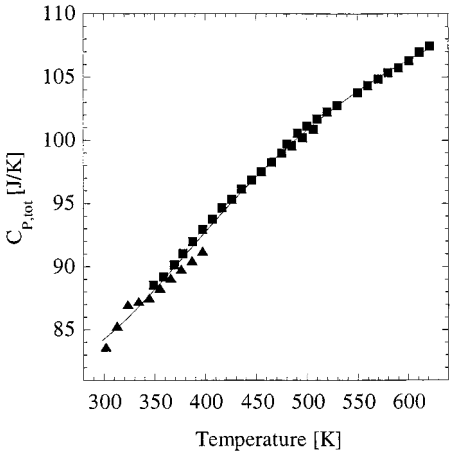

Figure 1. The total heat capacity of the calorimeter plus contents for the $CaMnO_{3-\delta}$(B) sample. Filled triangles are $C_{P,\mathrm{tot}}$ measured during oxidation, and filled squares are $C_{P,\mathrm{tot}}$ for the fully oxidized sample. The line represents the fitted $C_{P,\mathrm{tot}}$.

Table 3. Lattice Parameters of the Identified Phases in the Samples Studied[a]

sample	phases identified	lattice parameters		
		a (Å)	*b* (Å)	*c* (Å)
Partly Reduced				
$CaMnO_{3-\delta}$(A)	$CaMnO_{2.8}$	8.326 ± 0.003	–	7.469 ± 0.004
	$CaMnO_{2.75}$	5.347 ± 0.002	10.487 ± 0.002	7.466 ± 0.003
$CaMnO_{3-\delta}$(B)	$CaMnO_{2.5}$	10.221 ± 0.003	5.436 ± 0.002	3.747 ± 0.001
$Ca_2MnO_{4-\delta}$(A)	$Ca_2MnO_{3.5}$	5.300 ± 0.005	10.095 ± 0.004	12.247 ± 0.004
	Ca_2MnO_4	5.198 ± 0.006	–	24.113 ± 0.005
$SrMnO_{3-\delta}$(B)	$SrMnO_{2.5}$	10.768 ± 0.008	5.520 ± 0.004	3.814 ± 0.003
Reoxidized				
$CaMnO_3$(A)	$CaMnO_3$	5.292 ± 0.001	5.286 ± 0.002	7.463 ± 0.002
$CaMnO_3$(B)	$CaMnO_3$	5.277 ± 0.002	5.274 ± 0.003	7.467 ± 0.005
Ca_2MnO_4(A)	Ca_2MnO_4	5.183 ± 0.002	–	24.117 ± 0.002
$SrMnO_3$(B)	$SrMnO_3$	3.807 ± 0.001	–	–

[a] Oxygen stoichiometry $3-\delta$ and $4-\delta$ symbolizes the partially reduced samples before measurement, while stoichiometric samples (with oxygen stoichiometry 3 and 4) represent the samples after the oxidation measurement.

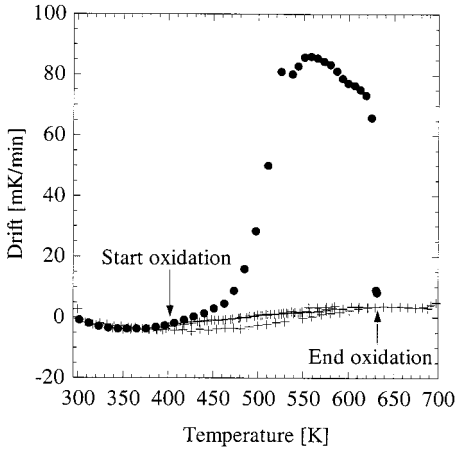

Figure 2. Temperature drift rate (TDR) curve for the $CaMnO_{3-\delta}$(B) sample. Filled circles are TDR measured during oxidation, while crosses are TDR measured for several different samples when no oxidation occurs.

drift rate is acceptable and does not lead to a larger uncertainty in the measured enthalpy of oxidation. A change in the set point of the PIDs changes the absolute value of the TDR and not the temperature variation of the TDR.

The oxygen content of the reduced samples and after the oxidation and the change in oxygen stoichiometry, $\Delta\delta$, are summarized in Table 2. The change in oxygen stoichiometry was calculated from the measured mass gained during the measurement of the enthalpy of oxidation. The oxygen stoichiometry of the reduced A samples was calculated from $\Delta\delta$ assuming the oxidized samples to be stoichiometric. These data are therefore not given with an uncertainty. Thermogravimetry and iodometry verified the stoichiometries of the reduced A samples. The oxygen stoichiometry of the reduced and oxidized B samples was determined by thermogravimetry and also confirmed by iodometric titration. The standard deviation ±0.01 given in the table is the highest possible for the B samples.

Table 3 summarizes the lattice parameters of all the phases observed before ($CaMnO_{3-\delta}$, $SrMnO_{3-\delta}$, and $Ca_2MnO_{4-\delta}$) and after ($CaMnO_3$, $SrMnO_3$, and Ca_2MnO_4) the oxidation. Two phases were observed in reduced $CaMnO_{3-\delta}$(A), $CaMnO_{2.8}$, and $CaMnO_{2.75}$.[15] The oxidized $CaMnO_3$(A) was a single-phase material.[11] The X-ray diffraction pattern of the $CaMnO_{3-\delta}$(B) sample showed the presence of small amounts of a secondary phase, $CaMn_2O_4$. $CaMn_2O_4$ has the spinel structure[26] and is stable under both oxidizing and reducing conditions, as confirmed by XRD. Since the oxygen stoichiometry of the secondary phase is constant, $CaMn_2O_4$ will not affect the weight gain measured during oxidation. The amount of $CaMn_2O_4$ was estimated by the following procedure. After oxidation the oxygen stoichiometry was found to be 2.990. The oxidized sample is assumed to consist of $CaMnO_{3.000}$ and $CaMn_2O_4$. Using this assumption and the weight gained during oxidation in the calorimeter, it was estimated that the $CaMnO_{3-\delta}$(B) and the $CaMnO_3$(B) samples contained 1.57 and 1.49 wt % $CaMn_2O_4$, respectively. The crystal structure of the main phase of the reduced $CaMnO_{3-\delta}$(B) sample and the oxidized $CaMnO_3$(B) sample were consistent with literature.[11,12] XRD of the reduced $Ca_2MnO_{4-\delta}$(A) demonstrated that the samples consisted of $Ca_2MnO_{3.5}$ and Ca_2MnO_4.[17] After oxidation these two materials were pure Ca_2MnO_4.[17] For the single phase $SrMnO_{3-\delta}$(B) sample, the reduced phase was indexed as $Sr_2Mn_2O_5$[18] and the oxidized sample as cubic metastable $SrMnO_3$.[19]

Discussion

Method. The accuracy of the temperature drift rate is assumed to be ±1 mK/min and of the heat capacity ±0.3%. This gives an uncertainty in $\Delta_{drift}H$ of ±235 J and in $\Delta_{total}H$ of ±70 J. The accuracy in the measurements of the sample mass is ±0.00001 g and of the mass change is ±0.00002 g. These are so small that they are not taken into the uncertainty calculations. The variations in the drift enthalpy and the total enthalpy give an uncertainty in the measured enthalpy of oxidation of maximum ±12 kJ/mol of O_2 or ± 3−4%. The accuracy and precision of the heat capacity determination for α-Al_2O_3 was found to be ±0.2%,[25] so an assumption of a slightly higher value of ±0.3% for the samples presented here is reasonable. For the temperature drift rate an accuracy of ±1 mK/min is a reasonable assumption, since it is on the same order of magnitude as the total change in the TDR during oxidation.

The enthalpy of oxidation can in addition to adiabatic calorimetry be measured by other methods such as solution or drop-solution calorimetry and differential scanning calorimetry (DSC). Solution calorimetry is an indirect method, where the enthalpy of oxidation has

(26) Riboud, P. V.; Muan, A. *J. Am. Ceram. Soc.* **1963**, *46*, 33.

to be calculated using a thermodynamic cycle and several enthalpies of solution measurements are involved. This has been done for several compounds such as $La_{2-x}A_xCuO_{4-y}$ (A = Ba, Sr, Ca, Pb),[27,28] $La_{2-x}A_xNiO_{4-y}$ (A = Ba, Sr),[29] and $La_{2-x}Sr_xCoO_{4-y}$[30]. Prasanna et al.[30] have shown that the error arising from the uncertainty in δy decreases with increasing δy but that the standard deviation of the mean is good and independent of δy. Measurements of the enthalpy of oxidation by DSC have until now not been published. A great challenge here will be the calibration, where one needs an almost identical powder as reference. An estimate of the uncertainty of this type of measurement is therefore not done.

Enthalpy of Oxidation. The $CaMnO_{3-\delta}$ sample studied here was not a single phase material but contained two reduced phases (see Table 3). We neglect the influence of the difference in the oxidation enthalpy between the two phases for this sample in the following discussion. The measured enthalpies of oxidation are summarized in Table 2. $SrMnO_{3-\delta}$ has the lowest and $Ca_2MnO_{4-\delta}$ the highest enthalpy of oxidation. The oxidation corresponds to the Mn^{3+} to Mn^{4+} transition in all the materials. In the pure Mn−O system the corresponding oxidation occurs between Mn_2O_3 and MnO_2. From drop-solution enthalpies of Mn_2O_3 and MnO_2 measured by Fritsch et al.,[31] the enthalpy of oxidation of the binary manganese oxides was found to be −39.6 kJ/mol of Mn, or −158.4 kJ/mol of O_2. The magnitude of the oxidation enthalpy is far less than that for $CaMnO_{3-\delta}$, $Ca_2MnO_{4-\delta}$, and $SrMnO_{3-\delta}$. This means that the basic oxides (CaO or SrO) have a significant influence on the enthalpy of oxidation.

The effect of the basicity of CaO and SrO is examined by comparing the enthalpies of the following reactions:

$$CaO + MnO_2 = CaMnO_3 \quad (2)$$

$$CaO + {}^1/_2Mn_2O_3 = {}^1/_2Ca_2Mn_2O_5 \quad (3)$$

$$SrO + MnO_2 = SrMnO_3 \quad (4)$$

$$SrO + {}^1/_2Mn_2O_3 = {}^1/_2Sr_2Mn_2O_5 \quad (5)$$

The enthalpies of these four reactions are −89.0, −36.4, −99.8, and −66.1 kJ/mol of Mn, respectively. The enthalpies are obtained by a combination of the enthalpies of oxidation reported here and the enthalpies of formation of $CaMnO_3$ and $SrMnO_3$ (the metastable perovskite phase) reported by Rørmark et al.[22] These data demonstrate that the enthalpies of formation of the ternary oxides $A_2Mn_2O_5$ and $AMnO_3$ (A = Ca or Sr) increase with increasing basicity of A. The effect is more pronounced the lower the oxidation state of Mn is. These observations are also consistent with the analysis offered by Yokokawa et al.,[32] who found that the enthalpy of formation becomes more negative with an increasing Goldschmidt tolerance factor, t. The tolerance factors for $CaMnO_3$, $SrMnO_3$ [calculated with the coordination number (CN) of A equal to 12, CN of B equal to 6, and CN of oxygen equal to 6], $Ca_2Mn_2O_5$, and $Sr_2Mn_2O_5$ (calculated with CN of A equal to 10, CN of B equal to 5, and CN of oxygen equal to 6) are 1.004, 1.041, 0.939, and 0.986, respectively.

The enthalpy of oxidation is more negative for $CaMnO_{3-\delta}$ than for $SrMnO_{3-\delta}$ and cannot be rationalized in terms of the basicity of CaO and SrO. Considering that the $SrMnO_3$ perovskite is a cubic metastable phase, it could be expected to reduce more easily than the orthorhombic stable $CaMnO_3$. We found that the enthalpy of oxidation was most negative for $CaMnO_{3-\delta}$, with the lowest tolerance factor.

A higher exothermic enthalpy of oxidation was observed for $CaMnO_{2.53}$ compared to $CaMnO_{2.77}$ (Table 3). Generally, in binary M−O systems the enthalpy of oxidation decreases with an increasing valence for the M. The present data is in accordance with the prediction that an increasing number of oxygen vacancies in the sample will increase the energy needed to remove another oxygen ion.

Changing the A/B ratio, 0 → 1 → 2, increases the enthalpy of oxidation in the order −40 → −89 → −111 kJ/mol of Mn (MnO_2, $CaMnO_3$, Ca_2MnO_4). This can be understood in terms of the connectivity of the crystal structures. MnO_2 has the rutile structure and consists of chains of edge-sharing octahedra, where the octahedra in one chain share corners with octahedra in other chains.[33] $CaMnO_3$ is a 3D network of corner-sharing octahedra,[11] while Ca_2MnO_4 on the other hand has 2D layers of corner-sharing octahedra.[17] The enthalpy of oxidation becomes more exothermic when going from edge-sharing octahedra in MnO_2 to a 3D network of corner-sharing octahedra in $CaMnO_3$ and finally to 2D layers of corner-sharing octahedra in Ca_2MnO_4. Reducing the amount of edge- or corner-sharing octahedra stabilizes Mn^{4+}. This is in accordance with the increasing concentration of basic components with increasing A/B ratio, which also favors Mn^{4+}. Yokokawa et al.[34,35] have offered a review on thermodynamic data on binary and ternary oxides with perovskite related structures. The enthalpies of oxidation of binary and ternary vanadium oxides were given, and for these oxides the enthalpy of oxidation was more negative for the ternary oxides, in accordance with the present findings.

Mn_2O_3, which consists only of edge-sharing octahedra,[36] changes to MnO_2 (rutile structure), which consists of both edge- and corner-sharing octahedra. In the case of the oxidation of $Ca_2Mn_2O_5$ to $CaMnO_3$, $Sr_2Mn_2O_5$ to $SrMnO_3$, and $Ca_2MnO_{3.5}$ to Ca_2MnO_4, the absorbed oxygen fills up the empty oxygen sites, resulting in an oxidation of square pyramidal coordinated Mn^{3+} to

(27) Bularzik, J.; Navrotsky, A.; DiCarlo, J.; Bringley, J.; Scott, B.; Trail, S. *J. Solid State Chem.* **1991**, *93*, 418.
(28) DiCarlo, J.; Bularzik, J.; Navrotsky, A. *J. Solid State Chem.* **1992**, *96*, 381.
(29) DiCarlo, J.; Mehta, A.; Banschick, D.; Navrotsky, A. *J. Solid State Chem.* **1993**, *103*, 186.
(30) Prasanna, T. R. S.; Navrotsky, A. *J. Solid State Chem.* **1994**, *112*, 192.
(31) Fritsch, S.; Navrotsky, A. *J. Am. Ceram. Soc.* **1996**, *79*, 1761.
(32) Yokokawa, H.; Kawada, T.; Dokiya, M. *J. Am. Ceram. Soc.* **1989**, *72*, 152.
(33) Baur, W. H. *Acta Crystallogr.* **1976**, *B 32*, 2200.
(34) Yokokawa, H.; Sakai, N.; Kawada, T.; Dokiya, M. *J. Am. Ceram. Soc.* **1990**, *73*, 649.
(35) Yokokawa, H.; Sakai, N.; Kawada, T.; Dokiya, M. *J. Solid State Chem.* **1991**, *94*, 106.
(36) Geller, S. *Acta Crystallogr.* **1971**, *B 27*, 821.

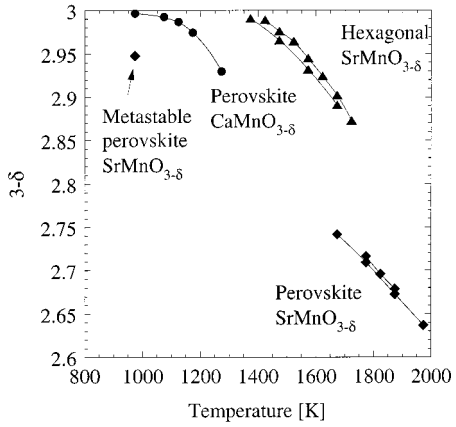

Figure 3. Measured oxygen nonstoichiometry of $CaMnO_{3-\delta}$[23] and $SrMnO_{3-\delta}$ in air.[19,20,23]

octahedral coordinated Mn^{4+}. The enthalpy of oxidation of the ternary oxides is found to be most negative.

Finally, an analogy is often that the change in Mn−O distance, Δ(Mn−O), is proportional to the enthalpy of oxidation, $\Delta_{ox}H$. From literature data[11,12,17−19] it can be seen that this expected correlation fails.

Thermodynamic Model for the Oxygen Deficiency of $AMnO_{3-\delta}$ (A = Ca or Sr). Negas et al. and Kuroda et al.[19,20] have measured the oxygen stoichiometry of both hexagonal and cubic (perovskite) $SrMnO_{3-\delta}$ as a function of the temperature at different partial pressures of oxygen. Corresponding data for $CaMnO_{3-\delta}$ has recently been reported by Rørmark et al.[23] Here we will compare these data with the thermodynamic models for these materials discussed below, using the measured enthalpy of oxidation of $AMnO_{3-\delta}$ (A = Ca or Sr) to estimate the redox properties of the materials. The reported oxygen nonstoichiometry for these samples in air is shown in Figure 3. The oxygen deficiency of perovskite $SrMnO_{3-\delta}$ is shifted to lower temperatures compared to $CaMnO_{3-\delta}$, in line with the smaller enthalpy of oxidation for $SrMnO_{3-\delta}$ (perovskite) than $CaMnO_{3-\delta}$. Note that the enthalpy of formation of $SrMnO_3$ is larger than for $CaMnO_3$ (eqs 2 and 4). The oxygen nonstoichiometry of the stable hexagonal Sr-
$MnO_{3-\delta}$ appears at significantly higher temperatures than for perovskite $SrMnO_{3-\delta}$. We therefore expect the enthalpy of oxidation of hexagonal $SrMnO_{3-\delta}$ to be far more exothermic than the corresponding value for perovskite $SrMnO_{3-\delta}$.

Two different models described in the literature will be used. One considers the manganese electrons as localized[37] and the other considers the Mn electrons as delocalized.[38]

In the case of the localized electron model, the Gibbs energy of formation of $AMnO_{3-\delta}$ can be expressed as a solid solution of the two ordered phases $AMnO_3$ and $AMnO_{2.5}$ ($A_2Mn_2O_5$).[37] The former phase contains only Mn^{4+}, whereas the latter contains only Mn^{3+}. The Gibbs free energy of formation of $AMnO_{3-\delta}$ is expressed for the solid solution as a function of δ, the oxygen non-stoichiometry:

$$\Delta_f G°(AMnO_{3-\delta}) = (1-2\delta)\Delta_f G°(AMnO_3) + 2\delta\Delta_f G°(AMnO_{2.5}) + (2\delta - 4\delta^2)\Omega_{Mn} + RT\left[(1-2\delta)\ln(1-2\delta) + 2\delta\ln(2\delta) + \delta\ln\left(\frac{\delta}{3}\right) + (3-\delta)\ln\left(1-\frac{\delta}{3}\right)\right] \quad (6)$$

where $\Delta_f G°(AMnO_{2.5})$ and $\Delta_f G°(AMnO_3)$ are the Gibbs energy of formation of the fully reduced and oxidized compounds. The entropic term in the equation (last term) corresponds to the configurational entropy of random distribution of Mn^{3+} and Mn^{4+} on B-sites in the perovskite structure and random distribution of oxygen and oxygen vacancies on the oxygen lattice sites. The nonideal behavior of the solid solution is introduced by a regular solution term, Ω_{Mn} for the interaction between Mn^{3+} and Mn^{4+}.[37]

The chemical potential of oxygen can be derived from expression (6):

$$\log P_{O_2}(\text{atm}) = \frac{4}{RT\ln 10}[\Delta_f G°(AMnO_3) - \Delta_f G°(AMnO_{2.5}) + (4\delta - 1)\Omega_{Mn}] + 4[\log(1-2\delta) - \log(2\delta)] - 2\log\left(\frac{\delta}{3-\delta}\right) \quad (7)$$

where

$$\Delta_f G°_m(AMnO_3) = \frac{1}{2}\Delta_f G°(A_2Mn_2O_5) + \Delta_{ox}H° - T\Delta_{ox}S° \quad (8)$$

and

$$\Delta_f G°_m(AMnO_{2.5}) = \frac{1}{2}\Delta_f G°(A_2Mn_2O_5) \quad (9)$$

The difference in free energy of formation between the end members of the solid solution can be represented by the observed enthalpy of oxidation (Table 1) and an estimate for the entropy of oxidation for the reaction

$$^1/_2A_2Mn_2O_5 + {}^1/_4O_2(g) = AMnO_3 \quad (10)$$

The entropy of the reduced compound is estimated by assuming $\Delta_r S° = 0$ for the reaction

$$Mn_2O_3 + 2AO = A_2Mn_2O_5 \quad (11)$$

The entropy of $AMnO_3$ is estimated as that for $AMnO_{2.5}$ times the atom ratio for $AMnO_3/AMnO_{2.5}$.

For the model with delocalized electrons on the Mn lattice the oxygen vacancies are assumed to be randomly distributed and noninteracting. The partial molar energy $H_{O_2}^{oxide}$ and entropy $S_{O_2}^{oxide}$ of oxygen was then expressed:[38]

$$H_{O_2}^{oxide} = 4(\Delta_{ox}H° - \delta H') \quad (12)$$

$$\boldsymbol{S}_{\mathbf{O}_2}^{\text{oxide}} = 4\Delta_{ox}S° + 2R\ln\left[\frac{\delta}{3-\delta}\right] \quad (13)$$

(37) Bakken, E. *Master Thesis (in Norwegian)*; University of Oslo, 1998.

(38) Lankhorst, M. H. R.; Bouwmeester, H. J. M.; Verweij, H. *J. Am. Ceram. Soc.* **1997**, *80*, 2175.

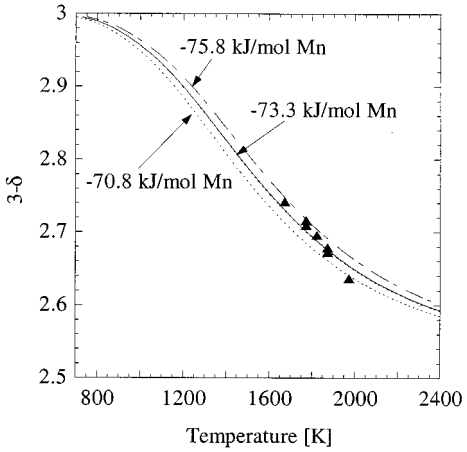

Figure 4. Oxygen nonstoichiometry for the metastable perovskite $SrMnO_{3-\delta}$ in air. The symbols are experimental data,[19,20] and the lines represent the ideal localized Mn electron model with $\Delta_{ox}H° = -73.3 \pm 2.5$ kJ/mol of Mn and the estimated entropy −32.3 J/(K·mol).

Using this, an expression for the chemical potential of oxygen can be written as

$$\log P_{O_2}(\text{atm}) = \frac{4}{RT \ln 10}[\Delta_{ox}H° - \delta H' - T\Delta_{ox}S°] - 2 \log\left(\frac{\delta}{3-\delta}\right) \quad (14)$$

where $\Delta_{ox}H°$ is the measured enthalpy of oxidation (Table 1), $\Delta_{ox}S°$ is estimated as described above, and H' is a constant.

The estimated oxygen defect concentration of the perovskite $SrMnO_{3-\delta}$ in air is shown in Figure 4 using the localized Mn electron model and $\Delta_{ox}H° = -73.3 \pm 2.5$ kJ/mol of Mn and the estimated entropy $\Delta_{ox}S° = -32.3$ J/(K·mol). As is seen, the measured enthalpy of oxidation gives a good estimate of the redox properties of the perovskite $SrMnO_{3-\delta}$. The oxygen nonstoichiometry estimated by the ideal model is close to the literature data,[19,20] but the measured nonstoichiometry seems to be more temperature dependent than that estimated.

In the following we will discuss how the parameters in the localized manganese electron model will influence the estimated defect chemistry. Generally, the oxygen defects are stabilized (shifted to lower temperatures) by a less exothermic oxidation enthalpy or more negative entropy of oxidation. A steeper slope for the nonstoichiometry versus temperature is obtained by a less exothermic enthalpy of oxidation with a simultaneous decrease in the entropy of oxidation. A better fit to the data was obtained by using an enthalpy and entropy of oxidation of respectively −120 kJ/mol of Mn and −58 J/(K·mol), as shown in Figure 5. These fitted thermodynamic parameters deviate from the measured enthalpy, −73 kJ/mol of Mn, and estimated entropy, −32 J/(K·mol). This shows that a free fit to the data gives a good estimate of the Gibbs energy but a large error estimate of the enthalpy and entropy.

The shape of the curve is more affected by the introduction of the nonideal term in eq 10. Generally, a negative deviation from ideality results in a steeper curve, while a positive deviation from ideality reduces the slope of the curve.

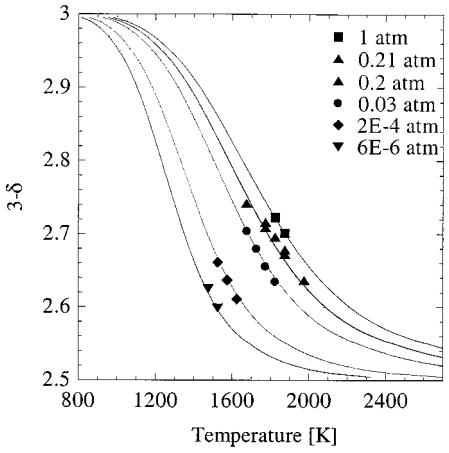

Figure 5. Oxygen nonstoichiometry for the metastable perovskite $SrMnO_{3-\delta}$ at different partial pressures of oxygen. The symbols are experimental data.[19,20] The solid lines are obtained by the localized model using an oxidation enthalpy and entropy of −120 kJ/mol of Mn and −58 J/(K·mol), respectively.

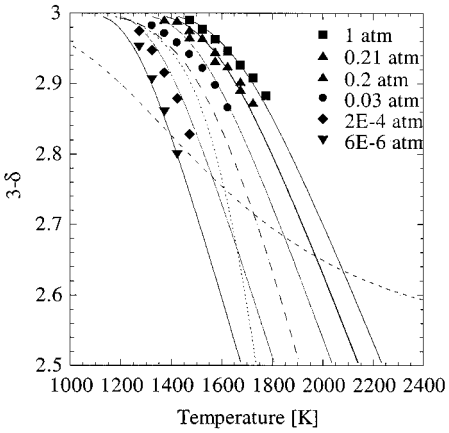

Figure 6. Oxygen nonstoichiometry for the hexagonal $SrMnO_{3-\delta}$ in air. The symbols are experimental data.[19,20] The short broken line represents the ideal localized Mn electron model. The dotted line is the ideal delocalized Mn electron model, and the long broken line is the delocalized electron model with $H' = -20\% \cdot \Delta_{ox}H°$ (perovskite) = +14.7 kJ/mol of Mn. The solid lines are obtained by the delocalized model using the following values for $\Delta_{ox}H°$, H', and $\Delta_{ox}S°$: −135 kJ/mol of Mn, 65 kJ/mol of Mn, and −68 J/(K·mol), respectively.

How do these models describe a crystal structure different from the perovskite structure they are developed for. As an example, let us discuss the hexagonal $SrMnO_{3-\delta}$, in which the crystal structure consists of pairs of face-sharing octahedra. The estimated oxygen defect concentration of the hexagonal $SrMnO_{3-\delta}$ in air using the localized electron model is shown as the short broken line in Figure 6. The initial reduction is 700−800 K higher in temperature than that for the cubic phase in air; see Figure 3. This indicates a significant difference in free energy between hexagonal and cubic $SrMnO_{3-\delta}$ and a significant difference in enthalpy of oxidation of reduced hexagonal and cubic $SrMnO_{3-\delta}$. The oxygen nonstoichiometry estimated with the measured enthalpy of oxidation of the perovskite hence lie much lower in temperature. Using the model for delocalized Mn electrons with the measured and estimated enthalpy and entropy of oxidation for the perovskite, the dotted line in Figure 6 is obtained. As seen from the figure, the slope is now too steep. Introducing the

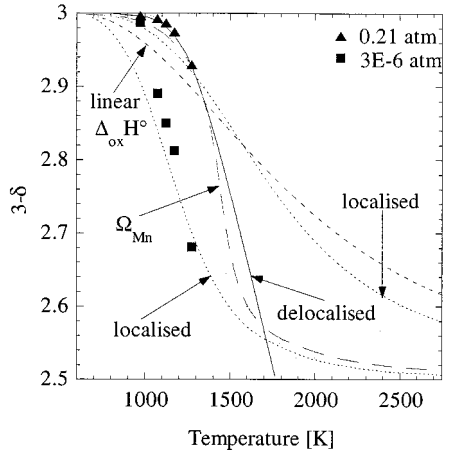

Figure 7. Oxygen nonstoichiometry for the perovskite $CaMnO_{3-\delta}$ in air and N_2 ($3\cdot\times 10^{-6}$ atm). The symbols are experimental data.[23] The dotted lines represent the ideal localized Mn electron model with $\Delta_{ox}H° = -85.1$ kJ/mol of Mn and an estimated $\Delta_{ox}S° = -34.6$ J/(K·mol). The short broken line (---) represents the ideal localized model in air with a linear variation of the enthalpy of oxidation from −105 kJ/mol of Mn at $3 - \delta = 3.0$ to −74 kJ/mol of Mn at $3 - \delta = 2.5$. The long broken line (− − −) corresponds to the localized model using $\Delta_{ox}S° = -46$ J/(K·mol) and $\Omega_{Mn} = +22$ kJ/mol. The solid line corresponds to the delocalized model with $\Delta_{ox}H° = -85.1$, $H' = 175$ kJ/mol of Mn, and $\Delta_{ox}S° = -51$ J/(K·mol).

oxygen dependent term in the partial energy decreases the steepness of the slope. This is shown as a long broken line in Figure 6, where H' is positive and given as 20% of the enthalpy of oxidation of the perovskite. A very good fit to the data was then obtained by increasing the enthalpy of oxidation to −135 kJ/mol of Mn, setting the constant H' equal to +65 kJ/mol of Mn, and increasing the estimated entropy to −68 J/(K·mol). These are rather large changes. The enthalpy associated with the phase transition from the metastable perovskite to the stable hexagonal $SrMnO_{3-\delta}$ was measured to −5.1 kJ/mol of Mn in N_2 and −7.1 kJ/mol of Mn in air by DTA.[23] These values are small compared with the increase of −62 kJ/mol of Mn of the measured $\Delta_{ox}H°$ (perovskite) for the fit of hexagonal $SrMnO_{3-\delta}$ in Figure 7. The enthalpy of formation of hexagonal $SrMnO_{3-\delta}$ can now be estimated. Using an average of 6.1 kJ/mol of Mn for the phase transition (perovskite to hexagonal $SrMnO_{3-\delta}$) and $\Delta_{ox}H° = -135$ kJ/mol of Mn, the enthalpy of formation from eqs 4 and 5 are −105.9 and −11.2 kJ/mol of Mn, respectively. This confirms that the hexagonal $SrMnO_3$ is more stable than the high-temperature perovskite phase. It also indicates that the perovskite $Sr_2Mn_2O_5$ is more stable than the reduced hexagonal phase.

An equal consideration is performed for the perovskite $CaMnO_{3-\delta}$. Figure 7 shows experimental data with the ideal localized electron model for $P_{O_2} = 0.21$ and $3\cdot\times 10^{-6}$ atm and $\Delta_{ox}H° = -85.1$ kJ/mol of Mn (the average of the two measured values) as dotted lines. The short broken line (---) represents the same model at $P_{O_2} = 0.21$ atm, but here the enthalpy of oxidation is given by a linear expression from −105 kJ/mol of Mn for $3 - \delta = 3.0$ to −74 kJ/mol of Mn for $3 - \delta = 2.5$. Although the model fits the data well, the steepness of the experimental data is significantly larger than the ideal model (Figure 7). The data obtained at $P_{O_2} = 3\cdot\times 10^{-6}$ atm will not be further discussed, since several phase transitions were observed in the measured temperature range.[23] For measurements done in air (0.21 atm of O_2) (Figure 7), it is seen that the ideal curve needs a steeper slope. For simplicity, all further calculations are done with an average of the enthalpy of oxidation of −85.1 kJ/mol of Mn. Notice that an even steeper slope is needed in the case of the linear dependence of $\Delta_{ox}H°$ on the oxygen nonstoichiometry (see Figure 7).

Introduction of $Mn^{3+} - Mn^{4+}$ interactions increases the curve gradient but moves the graph simultaneously to higher temperatures. This can be corrected by small changes in the estimated entropy, $\Delta_{ox}S°$. The Mn interaction parameter, Ω_{Mn}, was found to be 22 kJ/mol, and $\Delta_{ox}S°$ was found to be more negative than estimated. This result is shown as a long broken line (− − −) in Figure 7. As can be seen from the figure, the line is not curved enough at low oxygen deficiencies. The Mn interaction parameter contributes to the total enthalpy of oxidation (see eq 7). Introducing $\Omega_{Mn} = 22$ kJ/mol results in a variation of the total enthalpy of oxidation from −90.6 to −79.6 kJ/mol of Mn when the oxygen stoichiometry varies from 0 to 0.5, respectively. The delocalized electron model also results in a steeper slope for the oxygen nonstoichiometry versus temperature. Using this model for metallic conducting materials on the semiconducting $CaMnO_{3-\delta}$ in air gives a good fit (see the solid line in Figure 7). The experimental data is described by the model rather well using the following parameters: an unchanged enthalpy of oxidation, an oxygen stoichiometry dependent constant of 175 kJ/mol of Mn, and entropy of oxidation of −51 J/(K·mol).

As shown in the discussion above, the two simple models introduced here describe the defect chemistry of $CaMnO_{3-\delta}$ and $SrMnO_{3-\delta}$ fairly well. The partial free energy of oxygen for the localized model corresponds to the expression found by mass action type of consideration or point defect equilibrium. This is also the dominating model in solid state ionics. Using a point defect equilibrium the expression for the chemical potential for oxygen is obtained by assuming ideal and noninteracting point defects, and in most cases the concentration of defects is significantly less than in the two present cases. This work has shown that the measured enthalpies of oxidation give good estimates of the redox properties of $CaMnO_{3-\delta}$ and $SrMnO_{3-\delta}$. It is also seen that the enthalpy and entropy of oxidation of the best fit is not in good accord with experimental values, even though the estimate of the Gibbs energy is good. These observations call for more advanced models, which include terms for nonideal behavior and point defect interactions.

Conclusions

The present study has demonstrated that the enthalpy of oxidation of partly reduced perovskite-related materials is successfully obtained by in situ oxidation in an adiabatic calorimeter. The enthalpy of oxidation is sensitive to the concentration of basic oxides in the materials and the crystal structure. The enthalpy of oxidation of $CaMnO_{3-\delta}$ and $SrMnO_{3-\delta}$ has been used to estimate the oxygen nonstoichiometry by applying simple thermodynamic models.[37,38] The estimated nonstoichiometry is in good accord with experimental data.

The enthalpy of oxidation determined from a free fit to the experimental data does not agree with measured values. The present measurements are therefore of importance for the understanding of the thermodynamics of point defects. Simple models based on point defect equilibrium may give errors in the enthalpy and entropy of formation of defects, even though the models reproduce the free energy of formation. Finally, the present work has also demonstrated that oxygen nonstoichiometry in perovskites is determined by the relative stability of the two oxidation states of the transition metal and not the free energy of formation of the stoichiometric perovskite.

Acknowledgment. Financial support from the Research Council of Norway is acknowledged.

CM011050L